IAEA nuclear fusion

PAPER • **OPEN ACCESS**

Modeling of plasma facing component erosion, impurity migration, dust transport and melting processes at JET-ILW

To cite this article: I. Borodkina *et al* 2024 *Nucl. Fusion* **64** 106009

OPEN ACCESS
IOP Publishing | International Atomic Energy Agency
Nuclear Fusion
Nucl. Fusion **64** (2024) 106009 (14pp)
https://doi.org/10.1088/1741-4326/ad56a3

Modeling of plasma facing component erosion, impurity migration, dust transport and melting processes at JET-ILW

I. Borodkina[1,*], D.V. Borodin[2], D. Douai[3], J. Romazanov[2,4], E. Pawelec[5], E. de la Cal[6], H. Kumpulainen[7], S. Ratynskaia[8], L. Vignitchouk[8], D. Tskhakaya[1], A. Kirschner[2], E. Lazzaro[9], A. Uccello[9], S. Brezinsek[2,10], T. Dittmar[2], M. Groth[7], A. Huber[2], E. Thoren[8], G. Gervasini[9], F. Ghezzi[9], F. Causa[9], A. Widdowson[11], K. Lawson[11], D. Matveev[2], S. Wiesen[12], L. Laguardia[9] and JET Contributors[a]

[1] Institute of Plasma Physics of the CAS, U Slovanky 2525/1a, Prague 8 182 00, Czech Republic
[2] Forschungszentrum Jülich GmbH, Institut für Energie- und Klimaforschung—Plasmaphysik, Partner of the Trilateral Euregio Cluster (TEC), 52425 Jülich, Germany
[3] CEA, IRFM, F-13108 Saint-Paul-Lez-Durance, France
[4] JARA-HPC, Jülich Supercomputing Centre, Forschungszentrum Jülich GmbH, Jülich 52425, Germany
[5] University of Opole, Institute of Physics, Oleska 48, Opole, Poland
[6] CIEMAT, Avda. Complutense, 40, Madrid 28040, Spain
[7] Aalto University, Espoo, Finland
[8] Space and Plasma Physics—KTH Royal Institute of Technology, SE-10044 Stockholm, Sweden
[9] Istituto per la Scienza e Tecnologia dei Plasmi-CNR, Via R. Cozzi 53, I-20125 Milan, Italy
[10] Institut für Laser- und Plasmaphysik, Heinrich-Heine-Universität Düsseldorf, 40225 Düsseldorf, Germany
[11] Culham Science Centre, Abingdon, OX14 3DB Oxfordshire, United Kingdom of Great Britain and Northern Ireland
[12] DIFFER—Dutch Institute for Fundamental Energy Research, De Zaale 20, 5612 AJ Eindhoven, Netherlands

E-mail: borodkina@ipp.cas.cz

Received 12 February 2024, revised 21 May 2024
Accepted for publication 11 June 2024
Published 15 August 2024

Abstract

An overview of the modeling approaches, validation methods and recent main results of analysis and modeling activities related to the plasma-surface interaction (PSI) in JET-ILW experiments, including the recent H/D/T campaigns, is presented in this paper. Code applications to JET experiments improve general erosion/migration/retention prediction capabilities as well as

---

[a] See Maggi *et al* 2024 (https://doi.org/10.1088/1741-4326/ad3e16) for JET Contributors.
[*] Author to whom any correspondence should be addressed.

1741-4326/24/106009+14$33.00 Printed in the UK

various physics extensions, for instance a treatment of dust particles transport and a detailed description of melting and splashing of PFC induced by transient events at JET. 2D plasma edge transport codes like the SOLPS-ITER code as well as PSI codes are key to realistic description of relevant physical processes in power and particle exhaust. Validation of the PSI and edge transport models across JET experiments considering various effects (isotope effects, first wall geometry, including detailed 3D shaping of plasma-facing components, self-sputtering, thermo-forces, physical and chemically assisted physical sputtering formation of W and Be hydrides) is very important for predictive simulations of W and Be erosion and migration in ITER as well as for increasing quantitative credibility of the models. JET also presents a perfect test-bed for the investigation and modeling of melt material dynamics and its splashing and droplet ejection mechanisms. We attribute the second group of processes rather to transient events as for the steady state and, thus, treat those as independent additions outside the interplay with the first group.

Keywords: JET, impurity transport, physical erosion, beryllium, tungsten, isotope effect, plasma surface interaction codes

(Some figures may appear in colour only in the online journal)

1. Introduction

The JET tokamak is currently the only one capable of handling radioactive tritium (T) and equipped with a tungsten (W) divertor and beryllium (Be) main chamber (ITER-like wall, ILW [1]), which provides a unique and ITER-relevant environment for plasma-surface interaction (PSI) studies. Interaction of fuel species and impurities with plasma-facing components (PFCs) determines the erosion and lifetime of the PFCs [2, 3], fuel retention [4], dust formation [5] and transport of high-Z impurities to the core, affecting core impurity concentration and plasma performance [6, 7]. JET has recently featured experiments with hydrogen (H), deuterium (D) and tritium plasmas which were used for disentangling PSI processes (which are variously dependent on isotope plasma content), validating PSI and edge plasma codes and extrapolating predictions to ITER [8]. Numeric modeling of the mentioned processes and their interplay is a crucial tool for realistic and physically sound estimates of the lifetime expectations and performance of metallic PFCs in JET conditions relevant for ITER and DEMO.

An overview of the modeling approaches, validation methods and recent main results of analysis and modeling activities related to the PSI studies in JET experiments, including the recent H/D/T campaigns, is presented in this paper. Code applications to JET experiments improve general erosion/migration/retention prediction capabilities as well as various physics extensions like the treatment of dust particle transport and the detailed description of disruption-induced melting and splashing of PFCs at JET. The main erosion mechanisms relevant for a steady state phase of the ITER pulse (as extrapolated from JET) are the physical and chemically assisted physical sputtering (PS and CAPS) of PFCs by plasma ions and impurity ions, including seeded ions and eroded ions and resulting in self-sputtering; the charge exchange neutrals (CXN) also significantly contribute into erosion in diverted pulses [9]. Validation of the PSI and edge transport models taking into account various effects (isotope effects, first wall geometry, self-sputtering, thermo-forces, PS and CAPS, decay of W and Be hydrides in plasma) using data across JET experiments is very important for predictive simulations of PFC erosion and impurity migration in ITER. Moreover, our understanding of Be erosion and migration may be used to predict the behavior of low Z impurities in full-W devices, still containing boron, as boronization is typically required for wall conditioning in full-W [10]. Safety issues related to the release of debris from dust or droplets from the vessel's first wall are also crucial for the ITER operation. It is foreseen that the major contributor to the Be dust production in ITER will be a droplet ejection from melt pools induced on PFC surfaces during disruptions [5]. JET presents a perfect test-bed for the investigation and modeling of melt material dynamics, its splashing and droplet ejection mechanisms. It should be mentioned that the dust formation, splashing and dynamics of melt layers are characteristic for the disruptions and other transients (flaking, runaways, etc) rather than the steady-state plasma where PS and CAPS, redeposition, fuel implantation and outgassing etc are determined. Thus, these two groups of processes, both essential for the total PSI picture in JET and ITER, can fortunately be treated as somewhat decoupled. A short description of the codes used in the current plasma edge and PSI studies is presented in table 1.

The paper is organized as follows. Coupling between edge transport and PSI codes for an integrated simulation of PFC erosion, impurity migration and dust transport is presented in section 2. The main results of Be and W erosion and migration studies at JET are briefly summarized in this section, particularly describing the effects of isotope mass and edge-localized modes (ELM) on erosion, the CAPS contribution to Be sputtering and surface roughness effects. Spectral modeling of relevant diatomic molecules is presented in section 3. Section 4 contains the main results of the full kinetic modeling of JET SOL with a different D/T mixture. The approaches for macroscopic melt layer dynamics and splashing modeling are described in section 5. An investigation of the impact of the vertical displacement event (VDE) on the dynamics of droplets

Table 1. The overview of the codes used in the plasma edge and PSI modeling presented in this paper.

Code type	Code names	Code objectives in PSI modeling
Plasma edge transport packages: fluid approach for charged particles iterative coupled with kinetic (Monte-Carlo) for neutrals	EDGE2D-EIRENE SOLPS-ITER (B2.5-EIRENE)	2D multi-fluid edge plasma transport simulations in the SOL and divertor providing the *ab initio* self-consistent plasma backgrounds (poloidal 2D-maps of the plasma parameters). Both the main fuel and impurities are followed. The wall geometry is reduced to the poloidal contour (no toroidal shaping).
PSI and impurity transport codes	ERO1.0 ERO2.0	3D Monte-Carlo trace-impurity code for the PSI (erosion, redeposition, etc) and the impurity transport in the SOL/divertor simulations. Trajectories are giro motion resolved, detailed 3D wall shaping and surface sheath effects are included. ERO2.0 is massively parallelized providing simulations on JET/ITER scale.
Binary-collision approximation (BCA) Monte-Carlo plasma-facing surface code	SDTrimSP	Physical sputtering, deposition and reflection parameter calculation (yields, angle and energy distributions, etc)
Particle-in Cell codes	SPICE2 BIT1	Full kinetic codes for the resolved plasma transport simulations in the sheath at the vicinity of PFCs Full kinetic plasma, impurity and neutral transport for simulating a single flux tube in the SOL
Coupled core-edge suit of codes	JINTRAC	Combination of the core codes with the EDGE2D-EIRENE SOL/edge code for the integrated simulation of PSI and impurity transport to the core
Multiphase Navier-Stokes coupled with heat transfer	ANSYS FLUENT (specialized set-ups)	Simulations of small-scale dynamics and splashing of molten PFC material
Heat transfer coupled with the shallow water Navier-Stokes	MEMOS-U	Simulations of large-scale melting and macroscopic melt motion, able to reproduce the observed surface deformation
Dust dynamics code with electron/ion microphysics	MIGRAINe	Simulations of dust transport, survivability and accumulation sites in fusion reactors
Semi-analytic code compatible with EQDSK data	PELLYTIX	Simulation of pellet ablation and cloud deposition, including drift, using EQDSK magnetic configuration and geometry
Dust ballistic transport code	DUSTTRACK	Describing the transport of non-interacting spherical solid dust particles and molten droplets interacting with a non-stationary tokamak plasma configuration

is reported in section 6. Finally, the conclusions are drawn in section 7.

2. Be and W erosion and migration studies

Impurity transport and PSI codes are widely used for JET-ILW experiments modeling. In figure 1 an example of the iterative process between several edge transport and PSI code packages for simulation and validation of PFC erosion, impurity migration, and dust transport at JET-ILW is presented. Firstly, the plasma edge transport codes EDGE2D-EIRENE [11] and SOLPS-ITER [12] are used to produce 2D poloidal maps of plasma parameters, such as plasma and neutral densities and temperatures, particle and heat fluxes, neutral pressures, sources of particles, momentum and energy (distribution of ionization, dissociation and recombination events as well as spectroscopic and bolometric emission). The code outputs are validated by experimental data from spectroscopy, bolometry and other diagnostics in the JET tokamak, already producing lots of meaningful physics results. The produced plasma backgrounds are then implemented as input to the 3D giro-resolved PSI and impurity transport code ERO2.0 [13] for the simulation of Be and W erosion and transport or to the ballistic code DUSTRACK [14] for the dust transport modeling. ERO2.0 [13] is a linear Monte-Carlo PSI and impurity transport code that takes the first stage plasma background (BG) as input and provides synthetic diagnostics for sophisticated validation (figure 2), which can sometimes lead to a review of the taken BGs. ERO2.0 is widely used for tokamak [13] and stellarator plasmas [15] simulations. Further input data for the PSI codes are reflection and sputtering coefficients, which are

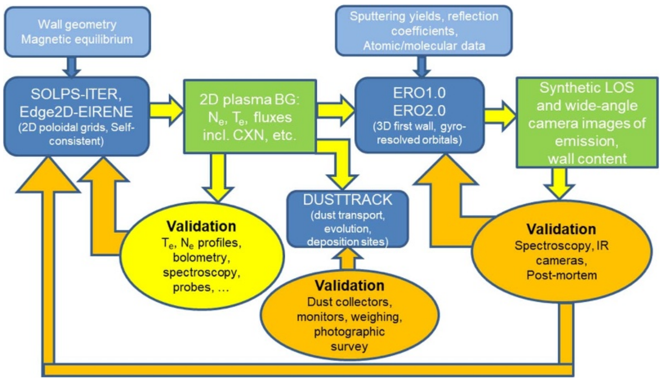

Figure 1. Interaction between the edge transport and PSI codes for simulation and validation of PSI processes.

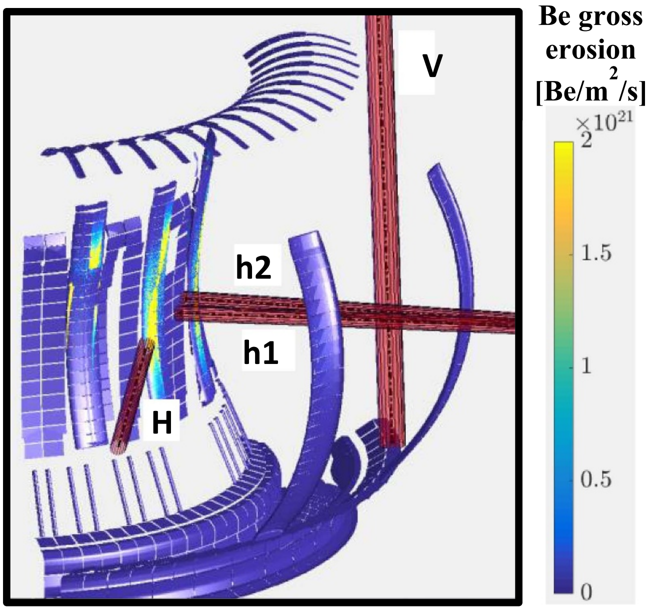

Figure 2. Incorporated into the ERO2.0 code JET passive spectroscopy sightlines of first wall areas of peak measured erosion (‘H’ pointed at inner wall guard limiter) and at other valuable measurement locations (h1, h2—horizontal view, V—divertor oriented sightline).

typically imported from the binary-collision approximation code SDTrimSP [16] or the molecular dynamics simulations. Using the set of the above mentioned codes, the H/D/T plasma isotope effects on Be and W erosion and impurity transport to the core plasma were analyzed for the first time at JET-ILW.

It was shown that the major part of W erosion by fuel species is due to ELMs resulting in highest transient hydrogenic particle fluxes to the divertor, whereas inter-ELM sputtering is dominated by Be impurities due to high impact energy threshold for W sputtering [9]. Typically, in the JET inter-ELM phase there are low electron temperatures in divertor ($\sim$30 eV) and thus low ion impact energies of fuel species ($\sim$150–200 eV), not sufficient for W sputtering by protons and deuterons. However, during ELMs, fuel ions are much more energetic in comparison with the background divertor plasma ions and cause W sputtering. Typical ion impact energies are higher than 1 keV. The ERO 2.0 code allows simulations of the material erosion by ions or CXNs, as well as impurity transport through the plasma considering atomic and molecular processes, secondary PSI processes like impurity re-deposition/re-erosion, detailed 3D wall geometry, machine-sized simulation volumes and sheath effects introduced by an analytical formula [17] based on particle-in-cell (PIC) modeling by SPICE2 [18] and BIT1 [19] codes. For the validation of the code output multiple diagnostic JET passive spectroscopy sightlines (shown in figure 2) are incorporated into the ERO2.0 code. In addition, ERO2.0 is capable of simulating images from 2D cameras with spectroscopic filters and even the temperature distribution along the first wall with impact of magnetic shadowing which is validated by infrared (IR) camera measurements [20]. ERO2.0 code was recently updated by adding important new physics and functionality into the code, as the homogeneous mixing model [21], the Guiding Centre approximation [22], the treatment of radial and parallel electric fields and thermoforces. To account for the influence of fuel content in the surface a set of Be sputtering data is parameterized using the so-called ‘ERO-max’ (assuming a clean Be surface) and ‘ERO-min’ (assuming 50% D content in the Be surface) assumptions for the PS yield fits. ERO2.0 simulations [13] revealed that ERO-min leads to a good agreement with measurements in the lower temperature range ($T_e \sim 5$ eV), where high D fluxes lead to a D-saturated Be surface. In contrast, ERO-max leads to a good agreement in the high temperature range ($T_e \sim 35$ eV), where outgassing and strong surface erosion lead to a cleaner Be surface. The earlier ERO2.0 simulations [13] of the 6 MW attached H-mode inter-ELM plasma are revisited and extended to H and T plasma with an updated set of sputtering and reflection data (by new SDTrimSP calculations), as well as including the mixing model for describing the Be/W dynamics in the divertor. Moreover, the recent simulations are time-dependent starting with the pure W divertor surface. The updated sputtering and reflecting yields are obtained by the SDTrimSP calculations, which are expected to be more realistic due to improved assumptions for surface binding energy and atomic densities [23]. The plasma background profiles and CX neutral fluxes from EDGE2D-EIRENE are used under the simplified assumption of having the same plasma conditions for H/D/T plasmas and only the sputtering/reflection data changing. ERO2.0 simulations presented here describe PFC erosion and impurity migration under inter-ELM plasma conditions where W sputtering is dominated by Be impurities due to a high impact energy threshold for W sputtering [9] in the case of H and D plasmas, whereas for T plasma, even the main T ions lead to non-negligible W erosion. The expected trend of both Be and W erosion increasing with isotope mass are shown in figure 3 where the erosion rates are integrated over the whole main chamber and divertor targets at JET under ERO-min and ERO-max conditions. W erosion dependence on isotope indirectly determined by the Be content in the plasma (the largest for T and the smallest for H) as W can be sputtered only by Be impurities in the inter-ELM phases. One can see that the ERO-min assumption (high fuel content in the wall) leads to lower

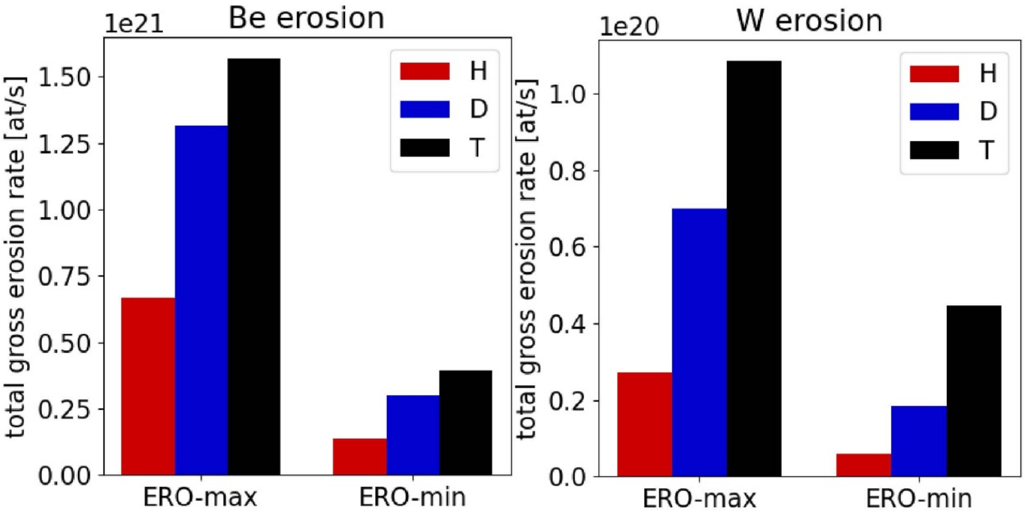

Figure 3. Integral Be and W total gross erosion rate under assumption of the pure Be surface ('ERO-max') and hydrated Be surface with an assumed 50% content of H/D/T ('ERO-min') in JET diverted plasmas.

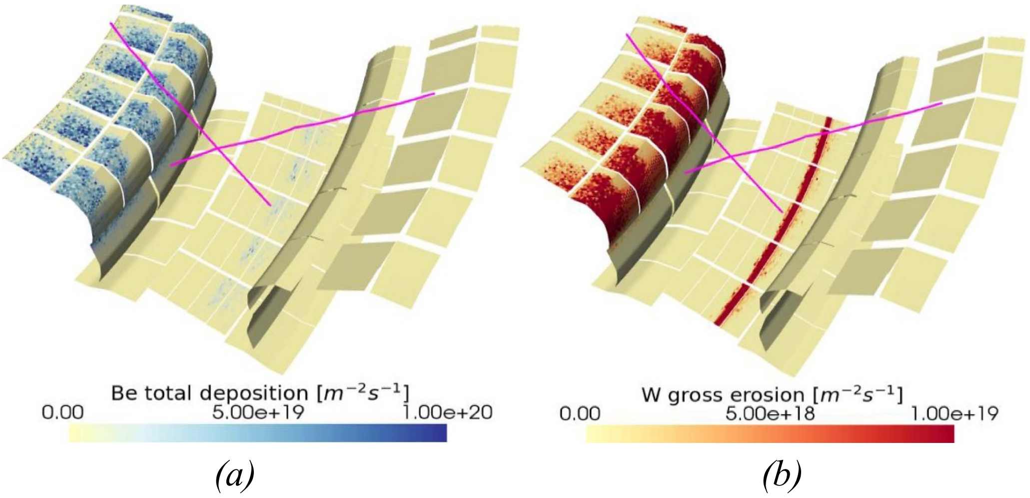

Figure 4. ERO2.0 simulation of (*a*) Be net deposition flux, (*b*) W gross erosion flux at JET divertor during the 6 MW H-mode inter-ELM T plasma exposure. Magnetic configuration is depicted by magenta separatrix lines.

sputtering coefficients. The ratio of Be sputtering for H:D:T is roughly proportional to the mass ratio 1:2:3, however for W the sputtering ratio is somewhat higher due to the combined erosion contribution of Be and main species, especially in T plasma. Figure 4 presents the 3D patterns of Be deposition and W gross erosion in the divertor for a T plasma after 1 s of exposure time, with the 'ERO-min' assumption showing that Be and Be hydrides predominantly migrate to the inner upper divertor resulting in the Be net deposition zones. This is well in line with a post-mortem analysis which has revealed Be deposits of several μm thicknesses in that region [24]. Moreover, post-mortem analysis of JET PFCs after two ILW campaigns revealed that fuel retention due to co-deposition with Be at the baffle of the inner divertor is the largest contribution (46%) to fuel retention in the PFCs [24], which must be kept below the safety limit in ITER. Diverted plasmas with the Inner Strike Point (SP) raised as close as possible to the inner baffle were successfully used for fuel removal from the thick co-deposited Be layers there [25].

Migration of Be and Be hydrides into the boundary of diverted plasmas largely determines the W erosion in inter-ELM conditions, which results in the W gross erosion patterns similar to the Be patterns, which could be seen in figure 4. Be migration initially leads to high W erosion in the inner divertor tiles. With longer exposure time the growth of a Be deposited layer leads to a reduction of W erosion there. The incorporation of additional sightlines to the ERO2.0 code (figure 2) reveals that the isotope effect is largely determined by the basic sputtering yield, however the specific sightline (local plasma parameters, Be/Be$^+$ ratio) and the line photon efficiency depending on T_e and n_e can also play a significant role. Figure 5 presents the comparison of the simulated Be II 527 nm line intensity of sputtered Be at the inner wall guard limiter from different

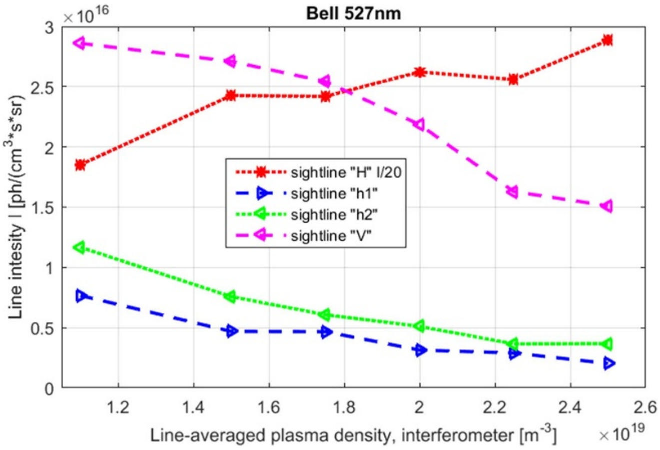

Figure 5. Simulated line intensities of the sputtered Be (BeII 527 nm line) at inner wall guard limiter from different JET passive spectroscopy sightlines incorporated into the ERO2.0 code as synthetic diagnostics (figure 2). The intensities show various trends by the plasma density scan measured by the interferometer vertically cross the plasma passing closely to its poloidal center.

sightlines at the limiter JET plasma conditions. The light intensity in various sightlines during the plasma parameter scan shows essential quantitative, and also even a qualitative difference (opposite trend on decreasing plasma density by increasing temperature).

Be 'inner wall guard' limiters (IWGL) in the main chamber of JET are the main source of Be impurities in the JET plasma. Effective Be sputtering yields were previously determined in D plasma from optical emission spectroscopy (OES) data via the ratio of the Be II 527 nm to the Balmer D_γ atomic line intensities using S/XB coefficients from the atomic data and analysis structure (ADAS)[13] relating spectroscopic intensities with the impurity influx (S/XB method [26]) in JET limited configuration pulses with the contact point at the high-field side midplane [27]. Recent JET experiments, similar to [4], aimed at repeating these pulses with H and T plasma, completing the study of the impact of the isotope mass on Be PS as well as CAPS and providing crucial input for validation of predictions of Be erosion and migration in ITER. Spectroscopic analysis evidenced that the effective Be PS increases with the isotope mass from H (red dots) to D (blue and cyan dots) to T (purple dots), as shown in figure 6. The values of the Be sputtering yield are higher than the SDTrimSP calculated [28] physical sputtering yields due to self-sputtering and CAPS. Validation of ERO 2.0 simulated Be sputtering yields by OES measurements evidenced that Be self-sputtering contributes to typically one third of the total Be erosion in plasmas in the limiter configuration [13]. It should be noted that SDTrimSP data do not capture CAPS effects. This may be improved in the future by combining BCA data with molecular dynamics simulations for the accurate analysis of Be sputtering by H/D/T projectiles. Recent experiments in H/D/T plasmas have confirmed that CAPS of Be responsible for the creation of Be hydrides contributes up to ~50% of Be erosion by D plasma at normal wall surface temperatures ~200 °C at JET-ILW Be limiters, while this erosion channel is completely suppressed at ~500 °C. This effect is related to the increased D outgassing from the surface and to the decreased D content in the surface layer. Figure 7 presents the integrated line intensities for selected Be I, Be II lines and BeD band characterizing the influx of those species from the inner wall guard Be limiter for H and D plasma. It was demonstrated that Be CAPS, characterized by beryllium hydrides BeH/D A → X band intensities, unlike the physical sputtering, is independent of the isotope, and the relative contribution of CAPS to erosion will be the largest in H plasma and smallest in T [29]. During experiments in nitrogen (N) seeded limiter JET discharges a strong reduction of the Be erosion of the limiter tiles was found [30]. Spectroscopy analysis showed that N seeding causes reduction of Be I and Be II as well as molecular BeD measured intensities which corresponds to CAPS suppression [30].

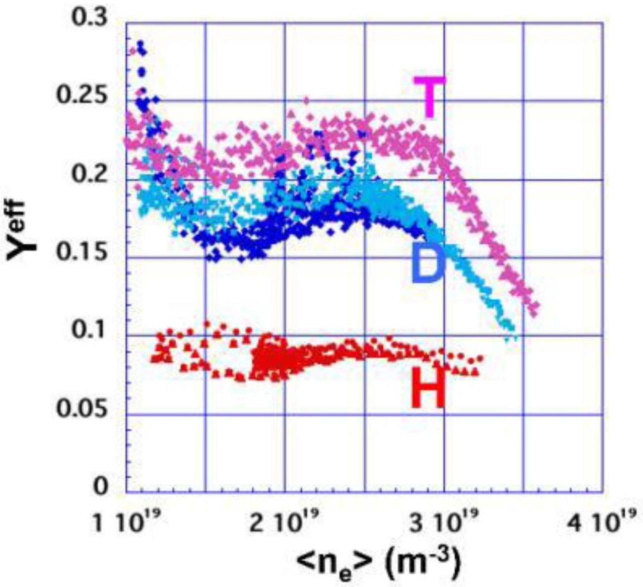

Figure 6. Effective Be physical sputtering yields in H, D and T limiter plasmas at inner limiter measured by visual range spectroscopy by the S/XB method.

JET experiments indicate that erosion of Be limiters can also be enhanced due to the increase of sheath potential introduced by magnetically connected ICRH antennas [31]. Simulations using the ERO1.0 [32] code with multiple model refinements and extensions such as magnetic shadowing, revisited separatrix location, inclusion of neutral fluxes and molecular release of Be, revised anomalous transport of ionized impurities as well as energy and angular distribution of background plasma flux qualitatively reproduced the experimental outcome [33]. A good agreement with the spectroscopically measured Be I and Be II signals was achieved under the assumption of 50% D content in Be surface layer, demonstrating that erosion increases with varying ICRH antenna's RF power.

Analytical assessment of ELM-induced W erosion in H and D plasmas was conducted reproducing the time evolution of

---

[13] Atomic Data and Analysis Structure (ADAS) (available at: http://adas.phys.strath.ac.uk).

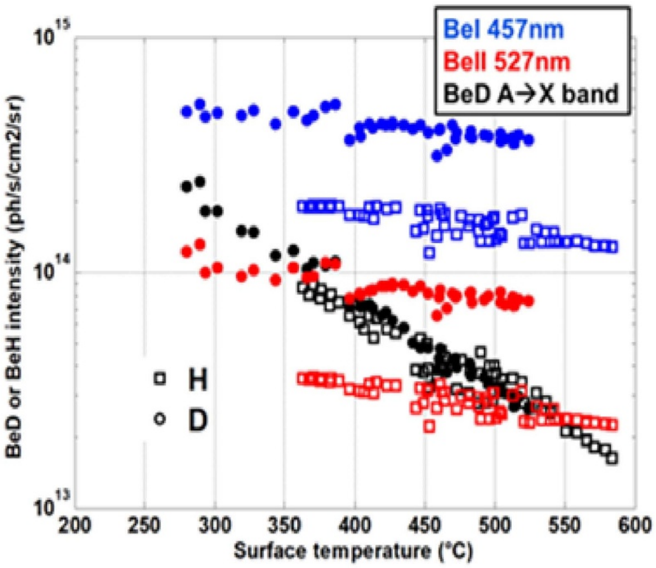

Figure 7. Measured line intensities of sputtered Be (ions, neutrals and BeD from CAPS) in H and D plasma.

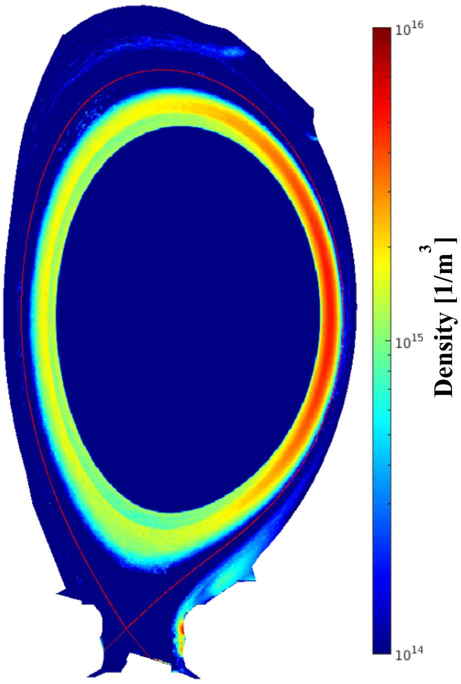

Figure 8. ELM-averaged W density distribution simulated by JINTRAC-ERO2.0 codes for JET ELMy H-mode plasma #94605. The separatrix is shown by red line.

pedestal n_e, T_e profiles, divertor heat and particle flux, Be II emission, and D-alpha emission during the ELM cycle [34]. Sheath effects influence ion impact energy and angle of incidence of sputtering ions, hence the effective erosion yields were shown to play an important role especially in inter-ELM conditions. A significant contribution ($\sim$85%) of Type I ELMs to the gross W sputtering in D plasma was confirmed by W I spectroscopy. The W gross erosion was predicted in dependence on fuel isotope mass, pedestal temperature and Be concentration in edge plasma under intra-ELM conditions. It was shown that W erosion per ELM induced by T was two times higher than by D at the same initial pedestal conditions. In this study, the fraction of Be ions was kept constant, whereas it might rise in addition during T plasma operation due to higher sputtering of Be from the main wall due to heavier charge-exchange neutrals [9]. The effect of plasma filaments appearing during ELMs on the JET Be limiter gross erosion was assessed for the first time based on an advective-diffusive model. The estimation of the ELM-induced Be erosion locally in the main chamber reveals a 30% increase in the Be sputtered flux under intra-ELM conditions for ELMs with $\Delta W_{\mathrm{ELM}} \sim 160$ kJ [35].

Penetration of high-Z W into the core leads to excessive core radiation and plasma contamination and could be reduced due to the high sputtering ion energy threshold of W by fuel species, the high probability of W prompt redeposition and divertor screening effects. Coupled JINTRAC [36] and ERO2.0 simulations of JET-ILW H-mode plasmas, including type-I ELMs, were conducted to predict the W density distribution in the JET SOL and core regions [37]. The plasma backgrounds obtained by JINTRAC code, taking into account cross-field drifts, were implemented into ERO2.0 code to model W erosion and edge transport. As a last step, the predicted W density at the pedestal top ($\rho = 0.9$) is used as the boundary condition for predictive W core transport simulations using JINTRAC. Assumption of Maxwellian CX neutral impact energy distribution was replaced by kinetic neutral energy spectra from EIRENE code allowing the consideration of non-Maxwellian high-energy tail due to charge-exchange atoms causing W erosion on non-plasma-wetted surfaces. The coupled simulations predict perfect screening of the W eroded at the divertor targets near the SPs during both the ELM and inter-ELM phases [38] due to high probability of W prompt redeposition, whereas erosion by CX atoms in conjunction with poor screening in the vertical outer divertor far SOL is predicted to be the dominant cause of W influx to the main plasma in both the ELM and inter-ELM phases. Figure 8 shows the synthetic map of the W density distribution averaged during inter and intra-ELM phases in JET predicted by ERO2.0 in D H-mode plasmas (JPN 94 605, $B_t/I_p = 2.5$ T/2.3 MA, $P_{\mathrm{NBI}}/P_{\mathrm{ICRH}} = 15$ MW/3 MW, $n_e = 6$–$7{\cdot}10^{19}$ m^{-3}). The presented simulations were validated by an integrated data analysis of soft x-ray, vacuum-ultraviolet, 2D bolometric, and effective charge measurements, also accounting for light and medium-Z impurities [39]. Based on the realistic boundary W concentration produced by ERO2.0, JINTRAC core transport modeling fitted to n_e, T_e, and T_i measurements successfully predicts the core W transport to be within a factor of 2 for H-mode ELMy JET plasma. Simulations for the T plasma predict that W erosion is 100% higher than in D in the inter-ELM phase and 120% higher in the ELM phase, predominantly due to the increased sputtering by T ions and CX atoms

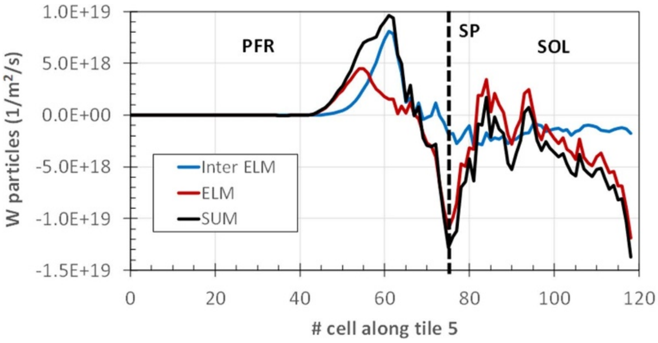

Figure 9. ERO1.0 simulated net erosion/deposition profiles of W outer tile 5 in JET-ILW in the private flux region (PFR) and SOL. Dashed line shows the position of the outer strike point (SP) on the horizontal tile.

[38]. It is found that the possible reasons for the discrepancy in the W emission ERO2.0 predictions include uncertainties in the background plasma conditions, the atomic data, in the tracking of metastable states (MS), assumptions on the sheath model and the sputtering angle distribution. The significance of MS effects for W was shown in a number of works [40], also the dedicated MS-resolved data set was implemented in ADAS database[14] for W. The modeling, however, depends on the initial population of the internal states in W just after sputtering which is an uncertainty [41].

Intra-ELM W sources were analyzed in the JET divertor demonstrating the dependence on the pedestal electron temperature and, correspondingly, on the ELM frequency. It was found that the ELM-induced W gross erosion rate (the number of eroded W atoms per second due to ELMs) increases initially with ELM frequency and reaches its maximum at ELM frequency 50–55 Hz followed by its reduction in the high frequency range. Strong decrease of in/out asymmetry of W erosion with ELM frequency and impact of magnetic configuration on divertor screening in type I ELMy H-mode plasmas were found evidencing the worst W screening by a factor of about 1.7 in the cases of inner and outer strike-points on corner horizontal W-coated target plates, compared to those with the outer strike-point on the semi-horizontal bulk-W divertor plate (the so-called tile 5) such as shown in figures 4 and 8 [42].

Net erosion is a crucial factor affecting the PFC lifetime prediction. The ERO1.0 simulations demonstrated a very low net erosion flux of W with a re-deposition fraction of more than 95% in the intra- and inter-ELM phases of the unseeded deuterium H-mode plasmas of the quasi-steady-state campaign C30C [9]. ERO1.0 simulations of dynamics of erosion and deposition profiles, taking into account the Be/W mixing model, determined the time evolution of surface Be and W concentrations of the tile 5 of JET divertor. Figure 9 shows the resulting net erosion/deposition profiles of W including the contributions of ELM and inter-ELM phases and the sum of both after averaging within 1 s considering the frequency and duration of the ELMs. It was found that the inter-ELM phases have significant contributions to the W erosion/deposition profiles (due to rather large electron temperature of 35 eV in between ELMs); however, when averaging within 1 s the net erosion from ELMs is about 2.5 times larger than that from the inter-ELM phases [43].

The main uncertainties regarding the erosion yields are connected with the surface state including saturation with fuel, oxidation state and roughness. The detailed ERO2.0 simulations were carried out to study the effect of roughness on the erosion of metallic surfaces. In [44] the developed ERO2.0 surface morphology model was applied to the JET-ILW W divertor consisting of smooth bulk W and rough W-coated CFC components to model the effect of surface roughness on sputtering and deposition in the JET-ILW divertor conditions. The simulations revealed that surface roughness leads to a reduction of net erosion by up to 50% depending on surface parameters and a decrease of the penetration length of sputtered particles into the plasma due to the more oblique sputtered angular distribution, which is in line with existing experimental observations.

3. Kinetic simulation of DT JET plasma

For the analysis of D-T experiments at JET it is important to simulate plasmas with different isotope ratios and predict the SOL plasma parameters. The full kinetic modeling of JET SOL with different D/T mixture was conducted by the PIC full kinetic massively parallel code for SOL modeling BIT1 [19]. The plasmas with three isotope D/T ratios as 25/75, 50/50 and 75/25 were simulated for neon (Ne)-seeded inter- and intra-ELM SOL phases. The simulation geometry corresponds to the magnetic flux tube limited by inner and outer divertor plates. Particle and heat sources near the outer mid-plane mimics cross separatrix transport. Simulations included electrons, D and T atoms and ions, and seeded impurity Ne. The ELM phase is simulated with increased particle and heat source strength. Further details of the kinetic SOL simulations can be found in [19]. Simulations of the JET cases were performed on the Marconi supercomputer and required 3–5 million CPU hours per case. It was shown that in the inter-ELM phase the divertor sheath parameters are nearly independent of the relative D/T concentration and the W sputtering from the divertors is caused mainly by the Ne^{++} ions (see figure 10). It should be noted that Be was not included in these simulations.

For the intra-ELM phase different ELM sizes and pedestal temperatures were considered with and without Ne seeding. To save the CPU time, we considered the first 80 μs after the ELM start, which seems to be sufficient to consider ELM buffering and W erosion. Simulations indicated no buffering of divertor power loads by the Ne impurity and qualitatively reproduced experimental results of W sputtering. In particular, it is shown in figure 11 that W sputtering increases and the inner/outer sputtering asymmetry decreases with increasing ELM size, which is in good agreement with the experimentally observed scaling [42]. Kinetic simulations of the sheath parameters during the ELM showed that the divertor T_e reaches $\sim$0.7–0.9 of the pedestal electron temperature for a short time

---

[14] Summers H.P. 2004 The ADAS User Manual, version 2.6 p 69 (available at: http://open.adas.ac.uk).

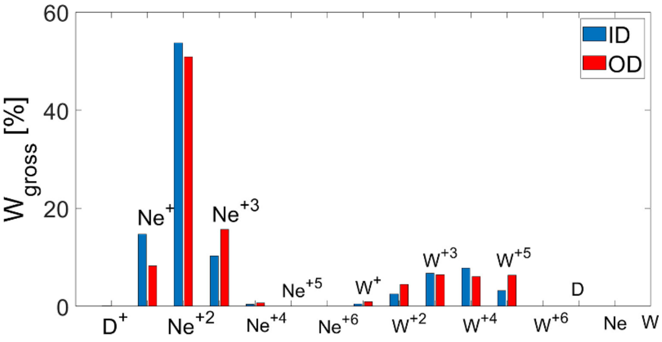

Figure 10. Relative W sputtering rates from the inner (ID) and outer (OD) divertor plates due to impact of different particles under inter-ELM conditions. Be was not included in the present BIT1 simulation.

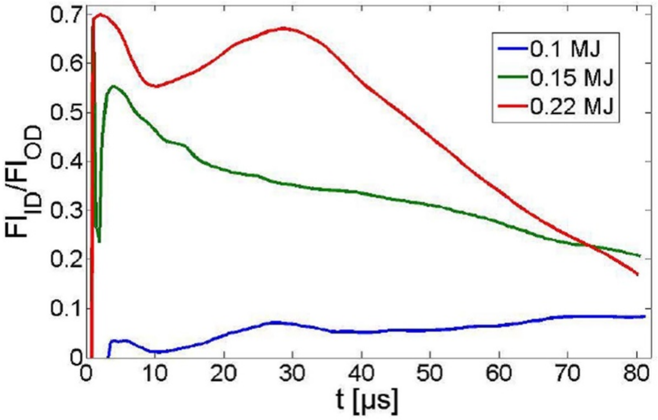

Figure 11. BIT1 simulated W sputtering asymmetry for different ELM size at JET.

interval ∼20 μs. One can conclude that there is no significant ELM electron-to-ion energy transfer in the SOL, which was later confirmed by revised experimental measurements [45].

4. Molecular spectroscopy simulations

The accurate description of the fuel in tokamak discharges affects a number of analyses including the investigation of molecular interactions with the plasma, the modeling of the plasma surface interactions which are important in understanding surface erosion and migration and the simulation of edge and divertor transport. Discrepancies have been found between the predictions of VUV Lyman series line intensities from well-established Collisional-Radiative (CR) models and their measurements on JET, firstly in D discharges, with similar discrepancies being evident when He was used as the discharge fuel. To gain an understanding a detailed study initially concentrating on He II is being carried out, thus avoiding some of the complexities found in D discharges. He fueled plasmas tend to have fewer impurities resulting in less complex spectra. Changes to the level populations due to interactions with D2 molecules are avoided and the effects of opacity resulting from the absorption of Lyman radiation are also expected to be smaller in He plasmas.

Extensive measurements of Lyman series line intensities have been made [46]; their ratios provide the most stringent test of the CR models, since the relative sensitivity calibration of VUV spectrometers is usually known more accurately than their absolute sensitivity calibration. For the spectral region encompassing He II Lyman series, the relative calibration of the JET spectrometers is known to within ±10%. Comparisons were made with two CR models, one based on the ADAS database[14] and the other on CHEM (Culham He Model [47]). The models show good agreement, for example, as can be seen in figure 12 for the Lyman alpha to beta ratios as a function of temperature for different plasma conditions. The discrepancies between the models and measurements are illustrated by the results (table 2) of minimizations of the function

$$\sum_i w_i \left(\frac{R_{\mathrm{mod},i} - R_{\mathrm{meas},i}}{R_{\mathrm{meas},i}} \right)^2,$$

where $R_{\mathrm{mod},i}$ is the modeled line intensity ratio for the ith ratio, $R_{\mathrm{meas},i}$ the corresponding measured line intensity ratio and w_i a weighting to account for differences in measurement accuracies. The summation includes all ratios for which there are both measurements and atomic data. In the minimization the electron temperature, T_e, the logarithm of the electron density, $\log_{10}(n_e)$ and the ratio of fully stripped to singly charged He ions, n^{2+}/n^{+}, were varied. Reasonable agreement is found only if the Lyman alpha to beta ratio is excluded from the minimizations. In these cases, the discrepancy for this ratio is typically × 3–5. It should be remembered that the Lyman alpha and beta lines account for ∼95% of the power radiated by the hydrogenic species. Opacity was considered as a possible cause of the discrepancy, but this explanation was found to be unsatisfactory and as yet the discrepancy is not understood.

The study did lead to a better understanding of opacity and this has led to a novel method for monitoring opacity in He plasmas [48]. Work is ongoing to assess D plasmas and initial results suggest that the discrepancies between modeled and measured line intensities range from values close to those found for He to a few examples for which there is reasonable agreement between theory and observations for all line ratios.

The edge plasma molecules and molecular ions strongly influence both the overall plasma behavior, fuel retention in the vessel walls and also their erosion, which contributes to the impurities permeating the pedestal and core plasma.

The influence of the molecular contribution on the plasma behavior is most visible in the divertor region. Modeling and spectral diagnostics of the detachment regime need to consider contributions of the molecules to the atomic ionization and recombination paths, which can for example, effect in the overpopulation of atomic levels leading to changes in specific D I radiation [49]. In JET divertor and midplane, the molecular spectra containing H_2, D_2, T_2 and mixed molecules were measured and analyzed [50] during attached and detached conditions.

Seeding impurities also introduces some molecular gases in the edge plasma. In the case of nitrogen, interactions with hydrogenic fuel contributes to the creation, via ND radicals, of

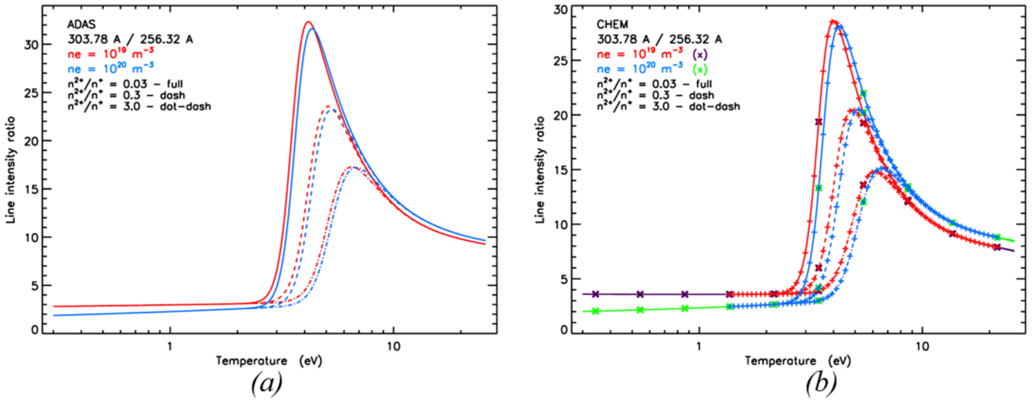

Figure 12. (*a*) ADAS Lyman alpha to beta line intensity ratios for two electron densities and three fully stripped He to He II ion density ratios. (*b*) CHEM Lyman alpha to beta line intensity ratios for two electron densities and three fully stripped He to He II ion density ratios. The data points from CHEM are shown, together with interpolated values.

Table 2. Results of minimization including and excluding the Lyman alpha/beta ratio.

Parameter	Initial value (Weight)	Upper and lower bounds (measurement)	Including alpha/beta		Excluding alpha/beta	
			CHEM	ADAS	CHEM	ADAS
T_e (eV)	4.0	0.2–25.0	4.01	4.25	4.41	4.95
$\mathrm{Log}_{10}(n_e)$ (m^{-3})	19.0	18.0–21.0	18.0	18.0	18.74	18.50
n^{2+}/n^{+} ratio	0.1	0.001–3.0	3.0	3.0	0.001	(0.3)[a]
Alpha/beta	(1.0)	(5.45)	6.14	5.85	27.9	23.6
Beta/gamma	(1.0)	(3.57)	2.26	2.21	3.98	3.57
Beta/delta	(0.9)	(9.15)	3.64	3.85	8.47	9.15
Beta/epsilon	(0.8)	(31.2)	5.37	—	29.0	—
Beta/zeta	(0.7)	(68.4)	7.68	—	70.1	—
RMS fractional difference			0.56	0.39	0.075	0.001

[a] In the ADAS case in which the Lyman alpha to beta ratio is excluded the n^{2+}/n^{+} ratio is fixed.

stable ammonia molecules. This effect is very detrimental as in tritium-containing plasmas it can lead to the production of tritiated ammonia and therefore the escape of tritium from the vessel containment. Measurements and analysis of molecular ND spectra together with RGA measurements of deuterated ammonia were performed in H-mode nitrogen-seeded JET plasmas [51].

In the case of erosion, a very important part is the production of metallic hydrides, especially BeH/D/T, which contribute to the wall erosion by CAPS. To improve the interpretation of spectroscopic measurements, serving either as input for edge codes or constraining erosion yield calculations, analysis of relevant diatomic molecule spectra has been performed. The main parameters describing the Be hydride behavior are the total intensity of the band and its shape, characterized by two main parameters—rotational and vibrational temperatures. Synthetic spectra calculated using theoretical data for the position and intensity of molecular lines from [52] of the three Be hydride isotopologues BeH, BeD and BeT are fitted to measured high-resolution spectra of the A 2Π to X 2Σ + Δ*v* = 0 transition at ∼500 nm. As can be seen in figure 13, the fits reproduce well the experimental spectra, yielding information about the rovibrational distribution and associated temperatures. Molecular parameters (including intensity [53]) are shown to depend on wall temperature, edge plasma density and hydrogen isotope used as a plasma fuel [54]. These results indicate the importance of including the

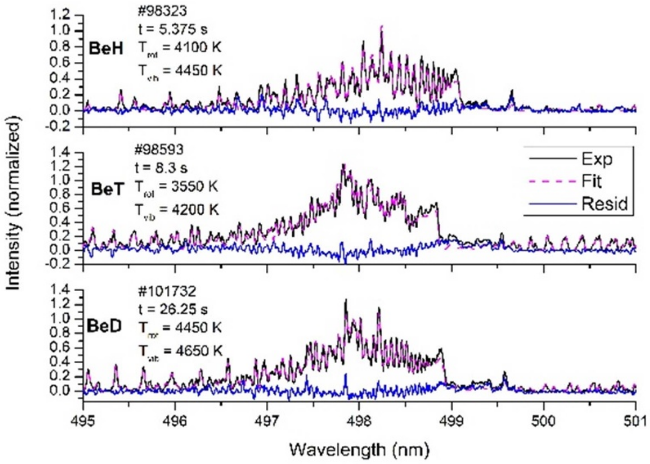

Figure 13. Experimental spectra and fits for three Be hydride isotopologues BeH, BeD and BeT and vibrational and rotational temperatures obtained from the fit [46].

rovibrational temperature in codes simulating CAPS in fusion devices.

5. Simulation of melt dynamics under transient events at JET-ILW

Extensive poloidal movement of the melt layer, ending with an upward going waterfall-like melt structure, is observed on the Be upper dump plates (UDPs) during the JET campaigns as a consequence of upward VDEs [55]. The large-scale Be UDP melting and macroscopic melt motion were successfully modeled with the MEMOS-U code [56, 57], while small-scale dynamics and splashing were simulated using customized ANSYS set-ups [57]. The coupling between fluid dynamics and heat transfer was included in the MEMOS-U code for the first time, which is necessary for scenarios where localized melt pools are bounded by progressively colder solid surfaces. It was shown that VDE heat fluxes continuously produce melt, which is then accelerated by Lorentz forces. The velocity and thickness of the moving melt layer, as well as the final surface deformation profile were predicted by taking into account the balance between the resolidification rate and the uninterrupted melt supply [56]. Macroscopic melt simulations described above were effective in predicting the overall amount of melt and its displacement at the Be UDP tiles, but they cannot account for instabilities and splashing. To address this issue, two-dimensional ANSYS Fluent Navier–Stokes hydrodynamic simulations of liquid Be layers flowing across a straight PFC edge have been carried out with varying melt depths and velocities in the ranges found in the MEMOS-U JET UDP macroscopic melt modeling. It is found that three main flow regimes exist that differ by the degree of attachment of the liquid on the downstream surface. Figure 14 presents the temperature distribution in three regimes. The parametric boundaries for the attached, intermediate and jetting regimes were determined, thereby providing a general stability criterion that can be applied to any transient melt event in fusion devices. Simulations of the melt dynamics in the intermediate regime confirm the stabilizing effect of melt re-solidification on plasma-shadowed surfaces downstream of the corner, where the relatively cold solid surface conducts thermal energy away from the liquid leading to a reduction of the downstream melt depth [57]. Good agreement with JET data regarding the melt ejection angles, morphological features of the frozen re-solidified metal layers and location of Be spatter on the vacuum vessel was obtained. Such modeling also provides input for droplet transport studies, in the form of initial sizes and velocities for droplets splashed from the molten layers under transient event conditions. This integrated modeling workflow, based on consecutive simulations of macroscopic melt motion, droplet production by splashing, and droplet transport in plasma, can be applied as a predictive tool for ITER, refining previous studies with the MIGRAINe code [58]. Droplet ejection is indeed foreseen as a major contributor to the Be dust mass production in ITER, along with the delamination of co-deposited Be layers, owing to the large droplet sizes [58–60].

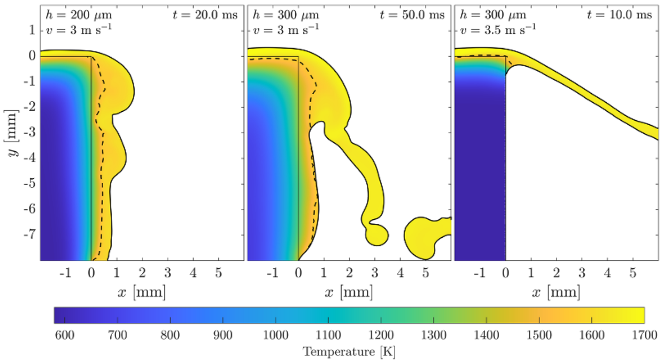

Figure 14. Example ANSYS results of temperature distribution in the attached (left), intermediate (middle) and jetting (right) regimes [56, 57].

6. Modeling of dust particle transport in JET-ILW plasmas

Dust production may pose safety and retention issues in ITER due to various reasons, such as remobilization of radioactive dust in the case of loss-of-vacuum accidents or a possibility of the explosion risk in the case of loss-of-coolant accidents, etc. For a long and safe tokamak operation it is necessary to control dust accumulation under the safety limits. For these reasons, investigation of the sources and the collection of dust in JET, supported by a systematic modeling of dust transport, is a crucial task for the preparation and monitoring of ITER. Dust transport codes are the main tool for predictive studies of dust production and migration to satisfy the limitations on the number of metallic dust particles inside the plasma chamber. Such simulations could provide an assessment of the in-vessel dust inventory evolution, accumulation sites, the droplet-to-dust mass conversion rate, etc [14, 59, 60].

In JET, experimental observations have provided evidence that the Be UDPs are the main source of debris due to ejection of droplets from the melting layer under strong heat loads during the unmitigated upward VDEs [61]. The investigation of Be droplet transport from the UDP of the JET-ILW tokamak during the stimulated unmitigated VDE of pulse #84832 was carried out using the specialized dust transport code DUSTTRACK capable of describing the full droplet dynamics in a non-stationary tokamak plasma configuration [62]. DUSTTRACK is a ballistic numerical code, which solves a system of non-linear, stiff ordinary differential and algebraic equations, describing the transport of non-interacting spherical solid dust particles and molten droplets in a non-stationary tokamak plasma configuration. The main outputs of the code are a 3D dust-particle trajectory in a tokamak plasma and the evolution in time of dust particle charge, temperature, mass and velocity. The general aim of this work was to connect the dust post-mortem data with the dust source and produce both

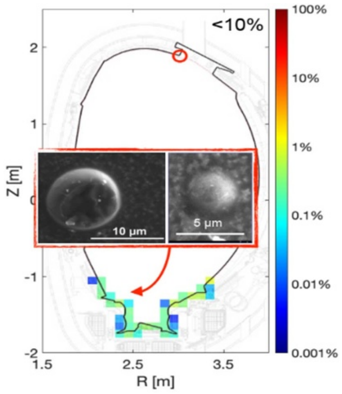

Figure 15. Example of DUSTTRACK results: distribution of deposited dust particles in the form of solid spherical droplets in divertor region.

qualitative and semi-quantitative statistical descriptions for the dependence of the deposition (state, location, size, impact speed) on the initial conditions. An approach based on JET experimental time-traces from different diagnostic tools has been developed to model the fast time-dependent background plasma, which was used as input in DUSTTRACK code modeling. The analysis of the time evolution of the main parameters of dust particles was carried out in the two phases of melt layer dynamics during VDE, at the beginning of thermal quench with the upward ejection toward the top of the vessel and during the current quench with a spray of droplets directly down. The upward simulation reproduced qualitatively the distribution of Be splats experimentally found at the top of the vessel near tile 8 of UDP on the low-field side. The downward simulations are in good qualitative agreement with observations from dust collection and sampling methods related to Be particles deposited on the outer wall and in the divertor region. DUSTTRACK downward simulations show that a significant percentage of droplets ablate near the ejection point (24%). The percentages of splats and solid spherical droplets are 37% and 39%, respectively. Distribution of dust deposits by type (spherical droplets or splats) and size was simulated in different locations of vessels, dust collectors, and mirrors, which could be compared with experimental findings. Figure 15 presents an example of modeling output: around 10% of the total ensemble of particles deposit in the form of solid spherical droplets with droplet size around 2–4 μm on the divertor tiles, which agrees with the measurements [63]. The DUSTTRACK results provide useful insight regarding the general physics influencing dust production and transport. The DUSTTRACK could be applied to the study of the dynamics of Be composite dust particles, such as Be oxides and hydroxides, found during post-mortem analysis of the UDPs in JET-ILW [64], which is again of interest for ITER.

During the JET-ILW campaigns, a systematic time correlation was observed for the evolution of the H-mode temperature and density pedestals in L–H–L transitions with the influx of W particulates across the separatrix, provided by high resolution Thomson scattering and vacuum UV diagnostic signals [65]. The methodology for modeling this effect was based on the use of an upgraded version of the ballistic code DUSTTRACK and a new code PELLYTIX [65] for dust ablation modeling. DUSTTRACK code modeling performed on the full non-uniform plasma parameter profiles from experimental data of the selected D and DT JET discharges demonstrated that the migration of W dust debris, from a divertor tile across the separatrix and the formation of a high Z_{eff} radiating layer, on time scales of few ms, is dominated by ballistic mechanisms, which depend on the dust particles initial momentum [63]. W influx effect on the pedestal density profile was well described by a ballistic ablation deposition model and could be significant if the size of W dust is more than 150 μm; however, it is not disastrous for tokamak operation if the total amount of W impurity mass is less than 15 mg.

7. Conclusions

This paper presents an overview of the main modeling and analysis approaches, the numerical edge transport and PSI codes and the achieved results related to Be/W first wall erosion, impurity migration, dust transport and dynamics of melting processes at JET with Be first wall and W divertor. The isotope dependence and the ELM effect on Be/W erosion, deposition and migration are discussed. The existing codes successfully reproduce the experimental measurements and can be used for predictive simulations for ITER.

Lessons related to PSI processes learned from the modeling and analysis activities at JET in view of ITER are summarized below:

(a) Physical sputtering was shown to be the main contributor to erosion and can be well reproduced by simulations provided that the underlying SDTrimSP sputtering yields are adopted to local conditions resulting in the effective yields [3].
(b) Be physical sputtering by H/D/T main plasma species has a strong isotope effect, however the CAPS contribution does not depend on the isotope mass.
(c) Molecular processes play a significant role in edge and divertor plasmas. Moreover, molecular spectral modeling suggests that the rovibrational temperature should be introduced as a parameter in SOLPS, Edge2D-EIRENE and similar modeling.
(d) Fuel co-deposition with Be at the top of the inner divertor is the largest contribution to fuel retention in the PFCs.
(e) The effective sputtering yields of metallic PFCs strongly depend on surface roughness, sheath effects and surface fuel content.
(f) ELMs mostly contribute to W erosion, however high prompt redeposition will allow to reduce W net erosion.
(g) Migration of W dust debris from a divertor tile across the separatrix affects the pedestal density profiles significantly if the size of the W dust is more than 150 μm.

In addition, it was demonstrated that OES is a powerful tool for validation of the simulated results. The large-scale melting of the Be UDP and macroscopic motion of the melt observed post-mortem in JET was successfully modeled with the MEMOS-U code while small-scale dynamics and splashing—with a customized ANSYS setup. The elaborated approach can be applied as a predictive tool for ITER, where the droplet ejection from melt pools induced on PFC surfaces during disruptions is foreseen as a major contributor to the Be dust production in ITER, along with the delamination of co-deposited Be layers.

Acknowledgments

This work has been carried out within the framework of the EUROfusion Consortium, funded by the European Union via the Euratom Research and Training Programme (Grant Agreement No 101052200—EUROfusion). Views and opinions expressed are, however, those of the author(s) only and do not necessarily reflect those of the European Union or the European Commission. Neither the European Union nor the European Commission can be held responsible for them. The results are obtained with the help of the EIRENE package (see www.eirene.de) including the related code, data and tools [66, 67]. The authors gratefully acknowledge the computing time granted by the JARA Vergabegremium and provided on the JARA Partition part of the supercomputer JURECA [68] at Forschungszentrum Jülich.

ORCID iDs

D.V. Borodin https://orcid.org/0000-0001-8354-1387
J. Romazanov https://orcid.org/0000-0001-9439-786X
E. Pawelec https://orcid.org/0000-0003-1333-6331
E. de la Cal https://orcid.org/0000-0001-8020-7682
H. Kumpulainen https://orcid.org/0000-0003-1301-0497
S. Ratynskaia https://orcid.org/0000-0002-6712-3625
L. Vignitchouk https://orcid.org/0000-0001-7796-1887
D. Tskhakaya https://orcid.org/0000-0002-4229-0961
A. Kirschner https://orcid.org/0000-0002-3213-3225
E. Lazzaro https://orcid.org/0000-0002-3291-8890
A. Uccello https://orcid.org/0000-0003-3044-1715
S. Brezinsek https://orcid.org/0000-0002-7213-3326
T. Dittmar https://orcid.org/0000-0002-4325-7979
M. Groth https://orcid.org/0000-0001-7397-1586
A. Huber https://orcid.org/0000-0002-3558-8129
G. Gervasini https://orcid.org/0000-0002-6732-7337
F. Causa https://orcid.org/0000-0003-0508-3100
A. Widdowson https://orcid.org/0000-0002-6805-8853
K. Lawson https://orcid.org/0000-0002-1251-6392
D. Matveev https://orcid.org/0000-0001-6129-8427
S. Wiesen https://orcid.org/0000-0002-3696-5475

References

[1] Brezinsek S. *et al* 2011 *J. Nucl. Mater.* **415** S936–42
[2] Brezinsek S., Borodin D., Coenen J.W., Kondratjew D., Laengner M., Pospieszczyk A. and Samm U. 2011 *Phys. Scr.* **T145** 14016
[3] Borodin D. *et al* 2019 *Nucl. Mater. Energy* **19** 510–5
[4] Brezinsek S. *et al* 2013 *Nucl. Fusion* **53** 083023
[5] De G. *et al* 2021 *Temmerman Nucl. Mater. Energy* **27** 100994
[6] Putterich T. *et al* 2013 *Plasma Phys. Control. Fusion* **55** 124036
[7] Dux R. *et al* 2009 *J. Nucl. Mater.* **390** 858
[8] Mailloux J. *et al* 2022 *Nucl. Fusion* **62** 042026
[9] Brezinsek S. *et al* 2019 *Nucl. Fusion* **59** 096035
[10] Krieger K., Balden M., Bortolon A., Dux R., Griener M., Hegele K., Laggner F., Rohde V. and Wampler W.R. 2023 *Nucl. Mater. Energy* **34** 101374
[11] Wiesen S. 2006 EDGE2D-EIRENE code interface report (available at: www.eirene.de/e2deir_report_30jun06.pdf)
[12] Wiesen S. *et al* 2015 *J. Nucl. Mater.* **463** 480
[13] Romazanov J. *et al* 2019 *Nucl. Mater. Energy* **18** 331–8
[14] Gervasini G., Lazzaro E. and Uccello A. 2017 *J. Fusion Energy* **36** 25–39
[15] Brezinsek S. *et al* 2022 *Nucl. Fusion* **62** 016006
[16] Mutzke A. *et al* 2019 Max-Planck-Institut für Plasmaphysik IPP-2019-0
[17] Borodkina I., Borodin D., Kirschner A., Tsvetkov I.V., Kurnaev V.A., Komm M., Dejarnac R. and Contributors J. 2016 *Contrib. Plasma Phys.* **56** 640–5
[18] Komm M., Gunn J.P., Dejarnac R., Pánek R., Pitts R.A. and Podolník A. 2017 *Nucl. Fusion* **57** 126047
[19] Tskhakaya D. 2017 *Plasma Phys. Control. Fusion* **59** 114001
[20] Romazanov J. *et al* 2017 *Phys. Scr.* **2017** 014018
[21] Navarro M. *et al* 2021 *63rd APS DPP Meeting* (*Pittsburgh, PA, 8–12 November 2021*) p O08.00007 (available at: https://meetings.aps.org/Meeting/DPP21/Content/4081)
[22] Rode S., Romazanov J., Reiser D., Brezinsek S., Linsmeier C. and Pukhov A. 2022 *Contrib. Plasma Phys.* **62** e202100172
[23] Romazanov J. *et al* 2024 *Nucl. Fusion* **64** 086016
[24] Widdowson A. *et al* 2017 *Nucl. Fusion* **57** 086045
[25] Matveev D. *et al* 2023 *Nucl. Fusion* **63** 112014
[26] Pospieszczyk A., Borodin D., Brezinsek S., Huber A., Kirschner A., Mertens P., Sergienko G., Schweer B., Beigman I.L. and Vainshtein L. 2010 *J. Phys. B: At. Mol. Opt. Phys.* **43** 144017
[27] de la Cal E. *et al* 2022 *Nucl. Fusion* **62** 126021
[28] Eckstein W. 2007 Sputtering yields *Sputtering by Particle Bombardment* vol 110 (Springer) pp 33–187
[29] Borodin D. *et al* 2022 *25th Int. Conf. on Plasma Surface Interaction in Controlled Fusion Devices (PSI-25)* (*Jeju, Korea, 13–17 June 2022*)
[30] Dittmar T. 2022 *25th Int. Conf. on Plasma Surface Interaction in Controlled Fusion Devices (PSI-25)* (*Jeju, Korea, 13–17 June 2022*)
[31] Klepper C.C. *et al* 2013 *J. Nucl. Mater.* **438** S594–8
[32] Kirschner A., Philipps V., Winter J. and Kögler U. 2000 *Nucl. Fusion* **40** 989
[33] Lasa A., Borodin D., Canik J.M., Klepper C.C., Groth M., Kirschner A., Airila M.I., Borodkina I. and Ding R. 2018 *Nucl. Fusion* **58** 016046
[34] Borodkina I., Borodin D., Brezinsek S., Kurnaev V.A., Huber A. and Sergienko G. 2020 *Phys. Scr.* **T171** 014027
[35] Borodkina I. *et al* 2017 *Nucl. Mater. Energy* **12** 341
[36] Romanelli M. *et al* 2014 *Plasma Fusion Res.* **9** 3403023
[37] Kumpulainen H.A., Groth M., Brezinsek S., Casson F., Corrigan G., Frassinetti L., Harting D. and Romazanov J. 2024 *Plasma Phys. Control. Fusion* **66** 055007
[38] Kumpulainen H. *et al* 2022 *Nucl. Mater. Energy* **33** 101264
[39] Sertoli M., Carvalho P.J., Giroud C. and Menmuir S. 2019 *J. Plasma Phys.* **85** 90585050
[40] Johnson C.A., Loch S.D. and Ennis D.A. 2020 *Plasma Phys. Control. Fusion* **62** 125017
[41] Eksaeva A., Marenkov E., Borodin D., Kreter A., Reinhart M., Kirschner A., Romazanov J., Terra A., Brezinsek S. and Nordlund K. 2017 *Nucl. Mater. Energy* **12** 253–60

[42] Huber A. *et al* 2020 *Nucl. Mater. Energy* **25** 100859
[43] Kirschner A. *et al* 2019 Modelling of tungsten erosion, transport and deposition in fusion devices *46th EPS Conference on Plasma Physics (EPS 2019)* (*Milan, Italy, 8–12 July 2019*) (available at: https://info.fusion.ciemat.es/OCS/EPS2019ABS/pdf/O2.107.pdf)
[44] Eksaeva A. *et al* 2021 *Nucl. Mater. Energy* **27** 100987
[45] Horacek J. *et al* 2023 *Nucl. Fusion* **63** 056007
[46] Lawson K.D. *et al* 2024 He II line intensity measurements in the JET tokamak *Plasma Phys. Control. Fusion* submitted
[47] Lawson K.D., Aggarwal K.M., Coffey I.H., Keenan F.P. and O'Mullane M.G. 2019 *J. Phys. B: At. Mol. Opt. Phys.* B **52** 045001
[48] Lawson K.D. 2024 *Private communication*
[49] Verhaegh K. *et al* 2021 *Nucl. Fusion* **61** 106014
[50] Pawelec E. *et al* 2022 *48th EPS Conf. on Plasma Physics* (*Maastricht, Netherlands, 27 June–1 July 2022*) (available at: http://ocs.ciemat.es/EPS2022PAP/pdf/O2.J501.pdf)
[51] Pawelec E. *et al* 2018 *J. Phys.: Conf. Ser.* **959** 012009
[52] Darby-Lewis D., Tennyson J., Lawson K.D., Yurchenko S.N., Stamp M.F., Shaw A. and Brezinsek S. 2018 *J. Phys. B: At. Mol. Opt. Phys.* B **51** 185701
[53] Brezinsek S., Stamp M.F., Nishijima D., Borodin D., Devaux S., Krieger K., Marsen S., O'Mullane M., Bjoerkas C. and Kirschner A. 2014 *Nucl. Fusion* **54** 103001
[54] Pawelec E., 2023 Chemically assisted physical sputtering of beryllium – temperature and density dependence in different hydrogen isotopes *PLASMA Conf.* (*Warsaw, Poland, 18–22 September 2023*) pp 1.1 (available at: https://plasma2023.ipplm.pl/images/2023/Book_of_abstracts.pdf)
[55] Jepu I. *et al* 2019 *Nucl. Fusion* **59** 086009
[56] Ratynskaia S., Thorén E., Tolias P., Pitts R.A., Krieger K., Vignitchouk L. and Iglesias D. 2020 *Nucl. Fusion* **60** 104001
[57] Vignitchouk L., Ratynskaia S., Pitts R.A., Lehnen M. and Contributors J. 2022 *Nucl. Fusion* **62** 036016
[58] Vignitchouk L., Ratynskaia S., Tolias P., Pitts R.A., De Temmerman G., Lehnen M. and Kiramov D. 2018 *Nucl. Fusion* **58** 076008
[59] Ratynskaia S., Vignitchouk L. and Tolias P. 2022 *Plasma Phys. Control. Fusion* **64** 044004
[60] Ratynskaia S., Bortolon A. and Krasheninnikov S.I. 2022 *Rev. Mod. Plasma Phys.* **6** 20
[61] Matthews G.F. *et al* 2016 *Phys. Scr.* **T167** 014070
[62] Uccello A. *et al* 2020 *Plasma Phys. Control. Fusion* **62** 064001
[63] Baron-Wiechec A. *et al* 2015 *Nucl. Fusion* **55** 113033
[64] Makepeace C. *et al* 2019 *Nucl. Mater. Energy* **19** 346–51
[65] Lazzaro E. *et al* 2022 *Nucl. Fusion* **62** 126037
[66] Reiter D., Baelmans M. and Börner P. 2005 *Fusion Sci. Technol.* **47** 172–86
[67] Borodin D.V. *et al* 2022 *Nucl. Fusion* **62** 086051
[68] Thörnig P. Jülich Supercomputing Centre 2021 *J. Large-scale Res. Facil.* **7** A182